CHAPTER-4

Solution-Processed Highly-efficient Organic-Inorganic nano-composite and Low- Voltage operated Field-effect Transistor based Hydrogen Sulfide Gas Sensor at sub-ppm Regime

4.1 Introduction 89
4.2 Experimental Section 92
4.2.1. Materials Used 92
4.2.2. Active and dielectric layer solution preparation 92
4.2.3. Device Fabrication 93
4.2.4. Surface Morphology 95
4.2.5. Dielectric film morphology 95
4.3 Sensing film morphology 96
4.4 Results and Discussion 98
4.4.1. Dielectric Properties 98
4.4.2. Electrical Properties 98
4.5 Gas Sensing Properties 101
4.5.1. Sensor Response 101
4.5.2. Transient Analysis and Repeatability 102
4.5.3. Selectivity 103
4.5.4. Relative Humidity and Stability 104
4.6 Gas Sensing Mechanism 105
4.7 Conclusion 109

The part of the work is adopted from-
V. K. Singh and V. N. Mishra, "**$HfLaO_x$ High-k Dielectric Based, Fully Solution Processed OFET H2S Gas Sensor at Sub-ppm Regime, Using Photoirradiated-SVA Annealed PCPDTBT/MoS_2 Nanocomposite Thin Film**," in ***IEEE Sensors Journal***, vol. 23, no. 20, pp. 24239-24246, 15 Oct.15, 2023, ***doi: 10.1109/JSEN.2023.331233.***

ABSTRACT

In chapter 3, various shortcomings of chapter 2 have been improved significantly. It is essential nowadays to develop low power consumption devices. In this regard, it is necessary to develop the sensor to operate at low voltage. To solve this problem, in this chapter the SiO_2 dielectric layer has been replaced by high-k dielectric material. Further, there is also scope left for improvement in all the sensing parameters obtained in chapter 3. Therefore, we have reported a highly efficient, low-voltage, and cost-effective H_2S gas sensor utilizing the nanocomposite thin film of conjugated organic polymer Poly[2,6-(4,4-bis-(2-ethylhexyl)-4H-cyclopenta [2,1-b; 3,4-b'] dithiophene)-alt-4,7-(2,1,3-benzothiadiazole)] (PCPDTBT) and inorganic material (MoS_2) as an active sensing layer. To enhance the molecular ordering of the polymer chains in composite solution, photoirradiation method has been employed. Facile, inexpensive, and solution-processed floating film transfer method (FTM) is used to fabricate the nanocomposite thin film of PCPDTBT/MoS_2. Furthermore, the state-of-the-art annealing method known as "solvent vapor annealing" provides im-proved crystallinity and excellent charge transfer throughout the polymer chain, which substantially enhances the gas sensing performance. High-k dielectric film of $HfLaO_x$ was deposited using the precursors of Hf and La, and spin coat-ing deposition method. The dielectric film exhibited a smooth, pin-hole free, and uniform nature with a very low rms roughness of 0.18 nm and excellent dielectric properties such as high bandgap (5.2 eV), low leakage current density (100 nA/cm^2 at -5 V), and high-k (24.8). To evaluate the thin film's electrical and gas detecting capabilities for harmful and dangerous H_2S gas, a top contact bottom gate (TCBG) organic field effect transistor (OFET) was fabricated. The device was exceptionally responsive to the

presence of hydrogen sulfide gas at concentrations even lower than 1 ppm and operated at room temperature (RT). The developed OFET device exhibits outstanding air stability, excellent response-recovery behavior, outstanding gas response repeatability, and a sensor response of 93.2% at 1 ppm exposure of H_2S gas. Response/recovery times are 4/55 seconds, respectively.

4.1 Introduction

OFETs (organic field-effect transistors) have made significant advancements and are of critical importance for applications in next-generation electronics. Power consumption is one of the key problems that requires being addressed for the industrialization of the OFETs. The development of OFETs necessitates an advancement of gate dielectric materials that are suitable for low power consumption. These materials must demonstrate exceptional electrical characteristics such as large capacitance, an exceptionally high breakdown strength, and a minimal leakage current density. Historically, the favoured gate dielectric material has been traditional silicon dioxide (SiO_2), but its relatively low dielectric constant does not meet the performance criteria for the aforementioned OFETs. OFETs with a low-voltage operation are required, and numerous progressively developed solutions have drawn a lot of interest from researchers in an effort to accomplish this. The source-drain current of a FET is dependent upon the oxide capacitance, generally described as:

$$C = k\frac{A\varepsilon}{d}$$

Where ε, d, k, and A are the free space permittivity, oxide thickness, relative dielectric constant, and area respectively. From the above equation, we can observe that the gate capacitance can either be increased by reducing the dielectric thickness or increasing the dielectric constant. Direct tunnelling phenomenon of the electrons causes the oxide

leakage current of the thin SiO_2 layer employed as the gate dielectric excessively high and exceeds 1 A/cm^2 at 1 V and 1.2 nm SiO_2 layer thickness [46]. Thus, the dissipation of the power at static conditions would be too high. Furthermore, the reliability of such thin film declines, and their fabrication becomes more challenging. As a result, SiO_2 has to be substituted. Tunnelling currents decrease rapidly as thickness increases. As a result, SiO_2 should be replaced with a layer of new material that is physically thicker and has a higher K value; this will maintain the capacitance while reducing the tunnelling current [48]. Furthermore, due to their high dielectric constant (K) and broad bandgap, hafnium (Hf), lanthanum (La), zirconium (Zr), aluminium (Al), and yttrium (Y) based oxides have been studied utilizing as the gate insulator by various scientific groups. Due to their excellent processing compatibility with organic and inorganic semiconductors, large conduction and valance band offset with respect to silicon substrate, and their significant chemical stability, Hf-based oxide dielectrics have been distinguished among the other oxides [47]. However, these oxide dielectrics, especially those based on Hf, have a propensity to crystallise swiftly and form grain boundaries that enhance the gate leakage current density. For the gate insulator to perform efficiently, it is essential to achieve amorphous insulator with high dielectric constant, thick, uniform, and pinhole-free film. Numerous scientific groups have utilized dopants like silicon (Si), yttrium (y), lanthanum (La), tantalum (Ta), and aluminium (Al) to increase the temperature at which crystallization takes place in order to produce the dielectric based on amorphous Hafnium. As a result, the Hafnium based dielectric's crystalline phase was prevented up to 900°C [46]. Due to their naturally lower dielectric constants than Hf, the majority of dopants, displayed the serious disadvantage of causing lowered dielectric constants. However, pristine LaO_x dielectric exhibits inhomogeneous morphology, highly hygroscopic nature, and

consists both amorphous and crystalline grains according to literature, but using as a dopant, La successfully controlled the Fermi level pinning without lowering the dielectric constant (K). Furthermore, due to La's high dielectric constant and significant conduction band offset, the Hf-based oxide with La doping had a noticeably low leakage current. However, only vacuum process technologies, such as chemical vapour deposition (CVD) and atomic layer deposition (ALD), which are restricted to large-area and low-cost deposition, were used to produce La-doped Hf-based oxide gate insulators. Therefore, we have deposited $HfLaO_x$ dielectric using solution-processed route in the present study. MoS_2 has gained significant scientific attention due to its favorable semiconducting properties in various optoelectronic applications such as gas sensing [97]. In addition, MoS_2 composites have shown sensitive behavior towards H_2S in some of the published literature [51][98]. The inorganic and polymeric components operate together as dopants for the counterparts, and enhance the electrical and gas sensing properties due to the synergistic effects of the constituent components, which enable to eradicate their intrinsic flaws while also taking into account the advantages of their inorganic and organic constituents in applications involving gas sensing [92]. That is why we have thoroughly investigated this composite material's electrical and H_2S gas-sensing properties. Because of their multiparametric analysis, sensitive detection, and compactness, the present work employs organic FET gas sensor [20]. The earlier discussed points motivated us to conduct the current investigation. Novelties of the current work include, utilization of the novel solution-processed method for the deposition of the $HfLaO_x$ dielectric layer, PCPDTBT/MoS_2 nanocomposite material as active gas sensing layer, and combination of photoirradiation of composite solution, floating film transfer deposition method, and solvent vapor annealing methods to improve device and gas sensing performance.

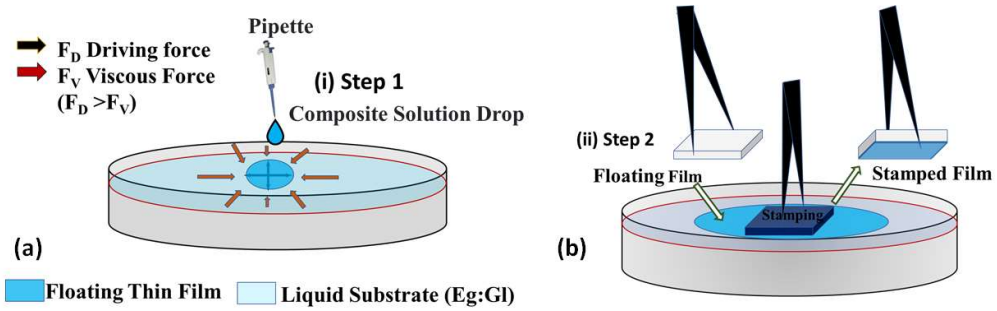

Figure 4.1 (a) Self-aligned floating film formation, (b) floating film stamping over HMDS-treated Si/HfLaOx dielectric film.

4.2 Experimental Section

4.2.1. Materials Used

The polymer PCPDTBT (average molecular weight Mw: 7 – 20 kDa) and MoS_2 nanoparticles (NPs) have been purchased from Sigma Aldrich (USA). Highly pure Hydrogen Sulfide gas (99.99%) has been purchased from Sigma Gases and Services Pvt. Ltd. (India). HMDS (hexamethyldisilazane), hafnium (IV) chloride, lanthanum acetate hydrate [$La(CH_3CO_2)_3 \cdot xH_2O$] (LaAc), methanol, ethylene glycol, glycerol, 2-ME (2 methoxy ethanol), and any other chemical used were purchased from Merck India Pvt Ltd. Without any further purification, all of the processing chemicals have been utilized.

4.2.2. Active and dielectric layer solution preparation

2 mg of MoS_2 nanoparticles and 10 mg of PCPDTBT were individually dissolved in 1 ml of chloroform solution. The solutions were continuously stirred at 900 rpm for 1.5 hours at RT. Additionally, a 5 w/v % PCPDTBT/MoS_2 nanocomposite solution was developed by mixing the two solutions. The nanocomposite solution was then agitated at 900 rpm for 60 minutes at RT to form a homogenous solution. Subsequently, the composite solution was photoirradiated (**Figure 4.2(c)**) by being subjected to UV light for 10 minutes

while being gently stirred. The vials containing the nanocomposite solution were placed underneath a custom UV lamp (P = 650 μW and λ = 365 nm) mounted over the magnetic stirrer. This method improves the molecular ordering and self-assembly of the PCPDTBT matrix by improving the π-π stacking and π-π interactions between the polymer chains [93], leading to high charge carrier mobility in the resultant PCPDTBT/MoS_2 composite. To deposit the $HfLaO_x$ dielectric thin film, a solution of 0.1 M hafnium chloride ($HfCl_4$) and lanthanum acetate hydrate [$La(CH_3CO_2)_3 \cdot xH_2O$] (LaAc) were prepared separately by dissolving in 2-ME. The solutions were kept on constant stirring at 1000 rpm, 50 °C for 5 hrs, resulting in a clear and homogenous solution. The solutions were filtered using a 0.2 μm PTFE syringe filter. Subsequently, both the solutions were mixed in a different vial tube in the ratio of 2:1, the mixed solution was rigorously stirred at 1000 rotation/min for 2 hrs at 50 °C to obtain a uniform clear solution and filtered by a 0.22 μm size poly-tetrafluoroethylene syringe.

4.2.3. Device Fabrication

The bottom-gate, top-contact OFET architecture used in the fabrication of the H_2S detector device is shown in **Figure 4.2(a)**. It utilizes polymer nanocomposite that serves as active sensing layer. The fabrication of the organic FET was done using the following process. The typical wet cleaning procedure is used to clean a p++ Silicon wafer. Further, to obtain uniform surface energy activated surface the cleaned substrate was treated with O_2 (oxygen) plasma for 5 minutes. Subsequently, the dielectric layer solution was spin-coated at 3000 rpm for 40 sec onto the Si substrate. After spin coating, the substrate was placed on a hotplate at 100 °C for 5 min. Finally, the substrate was annealed at the 500 °C temperature in an Argon glove box. The obtained thickness of the dielectric layer was

60 ± 3 nm (measured by Filmetrics F20-UV). Further, surface treatment of the Si/HfLaOx wafer was performed using the vapors of HMDS (hexamethyldisilazane) (~5 nm self-assembled monolayer) to obtain a surface which is hydrophobic in nature, and to passivate the trapping sites activated by the surface charge for better film adhesion.

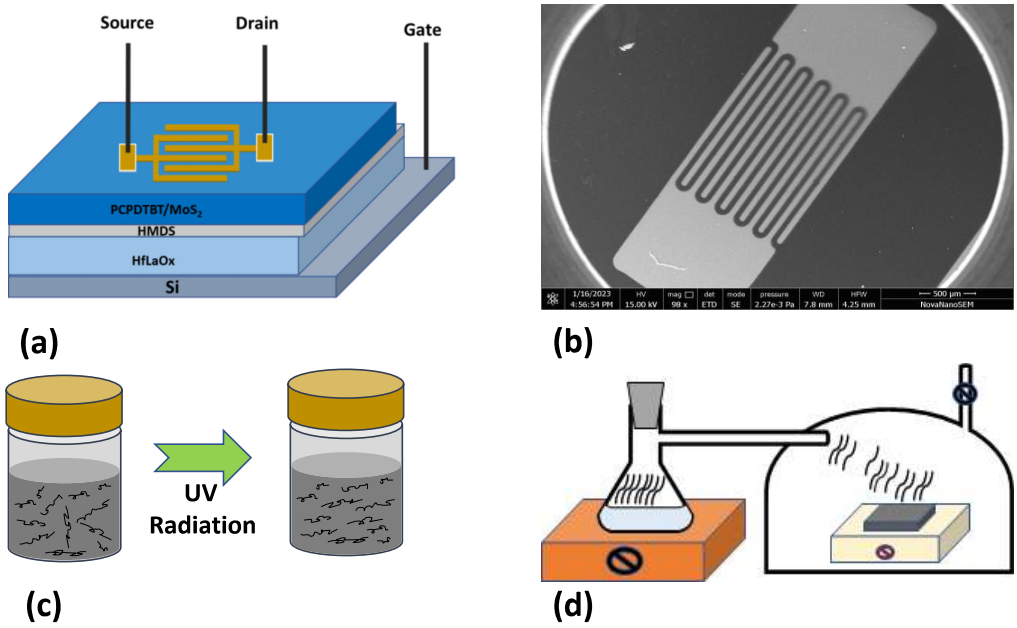

Figure 4.2 (a) Architecture of the fabricated sensor (b) Zoomed-in Device Image (c) Schematic of photoirradiation process (d) SVA method

Additionally, a small amount of the composite polymer solution was dropped onto a combination of the liquids Eg: Gl (3:1) (a hydrophilic liquid substrate). This combination was chosen since it has demonstrated films with the maximum anisotropy at this concentration [74]. A long thin floating film has been developed over the liquid substrate due to solvent's (chloroform) dynamic evaporation as shown in **Figure 4.1(b)**. Using a polarizer sheet, the orientated region of this film was identified and stamped onto the Si/HfLaOx substrate that was treated with HMDS. The samples were annealed at 60 °C for 30 min in an Argon glove box. Additionally, we performed solvent vapor annealing (SVA) on

the film for 1 hour using chlorobenzene (CB) vapor. The FTM-deposited substrate was put in a closed container with an entrance that has a valve that can open and close. The chlorobenzene solution was heated in a different airtight container until vapor production was constant. Chlorobenzene vapours then flowed for one hour to the substrate container's entrance with the aid of an airtight pipe (**Figure 4.2(d)**). After that, the HHV 12A4D thermal coating unit deposited 50 nm thick thermally evaporated gold (Au) source and drain electrodes at a constant 10^{-6} torr pressure.

4.2.4. Surface Morphology

NT-MDT, Model - NTEGRA Prima atomic force microscopy was used in tapping mode to assess the surface topography of the dielectric and polymer nanocomposite film.

4.2.5. Dielectric film morphology

A uniform and smooth surface morphology is a desired criterion for insulating materials used as gate insulator in electronic devices. The uniform surface of the insulating thin film decreases carrier scattering centers, prevent the growth of interface charge traps, and achieve high field-effect mobility, all of which are advantageous for enhancing the TFTs' performance. The surface morphologies of the prepared gate dielectric thin films are shown in **Figure 4.3**. The HfOx and HfLaOx films had smooth surfaces with RMS roughness values of 0.46 and 0.18 nm, respectively (**Figure 4.3(a) and (b)**).

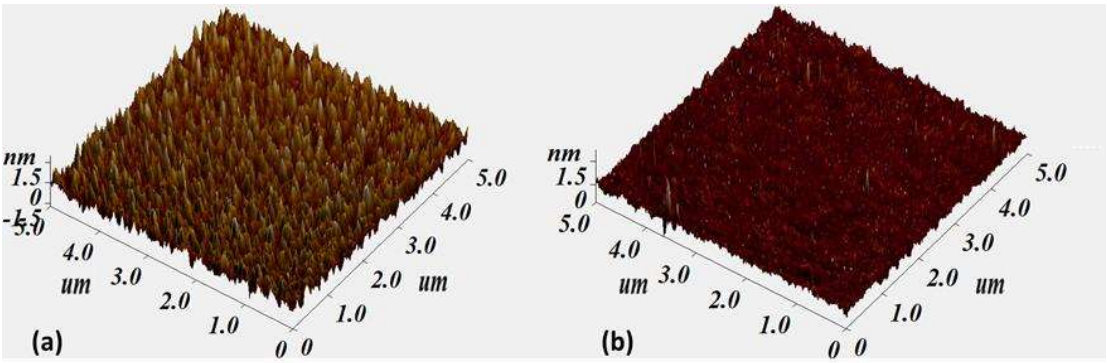

Figure 4.3 3-D AFM image of the (a) HfOx and (b) HfLaOx dielectric

The very smooth surface of the HfOx and HfLaOx dielectric films may have been caused by the annealing temperature being high enough to remove complicated ligands and create a dense network of metal-oxygen-metal connections. Crystallization is responsible for the greater RMS roughness of HfOx film compared with HfLaOx.

4.3 Sensing film morphology

Figure 4.4 displays AFM images of the thermally and photoirradiated-SVA annealed PCPDTBT/MoS_2 thin film that were scanned across a 3×3 μm^2 region.

Table 4.1 includes all of the retrieved parameters. For the Photoirradiated-SVA treated film, we can see that the grain size and length have significantly decreased, although the RMS roughness is somewhat increased. The polymer film's grain analysis, shown in **Figure 4.4(c) and (f),** shows that the photoirradiated-SVA treated film generated many more grain boundaries than the thermally annealed film because the latter had larger grains. Additionally, we can see that the Photoirradiated-SVA treated film has better aligned and connected grains by observing **Figure 4.4 (a), (c), (d), and (f).** As seen in **Figure 4.4(f)**, the linked neighboring grains improve the charge transport process by offering a better percolation channel for the charge transport throughout the active sensing layer [75]. Surface roughness and the number of grain boundaries are essential factors in the improved

gas adsorption (physisorption) process. Additionally, for a more effective charge transfer mechanism, the film's alignment and the grains' interconnections are essential. As previously stated, the above-mentioned characteristics have greatly improved, which has enhanced the physisorption and charge transport mechanism and increased sensitivity. The combined impact of the solvent vapor annealing process and floating film transfer deposition is responsible for all the advances in surface morphology that have been emphasized.

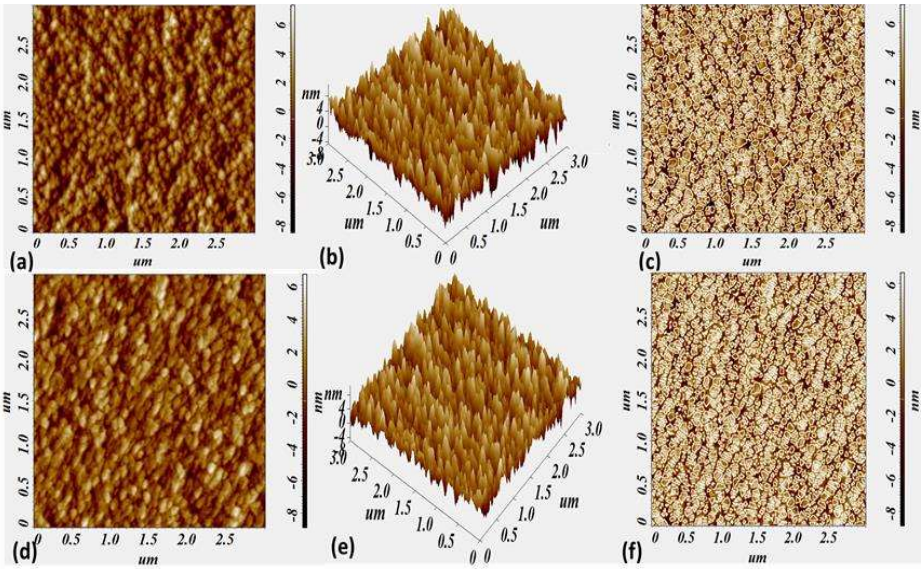

Figure 4.4 2-D, 3-D, and Grain analysis AFM image of the ((a–(c)) Thermally annealed PCPDTBT film and ((d)–(f)) Photoirradiated-SVA annealed PCPDTBT film, respectively.

Table 4.1 AFM Parameters for SVA and Thermally annealed PCPDTBT film

Parameters	Photoirradiated-SVA film	Thermally annealed film
RMS roughness (nm)	3.3	3
Average grain size (nm)	50	60
Average grain length (nm)	78	93

Additionally, by adjusting the liquid substrate's composition, temperature, and concentration, we were able to optimize the polymer film's thickness. First, we discovered that when the thickness is reduced, the sensitivity to certain film thicknesses increases before

gradually declining. This observed behavior is consistent with the published research.[68]. The Filmetrics F20-UV was used to measure the optimum film thickness, which was obtained ~20 nm.

4.4 Results and Discussion

4.4.1. Dielectric Properties

Figure 4.5(a) shows the corresponding capacitance–frequency characteristics of the HfLaOx dielectric. Capacitance characteristics were measured between the frequency range of 1 kHz and 1 MHz. The polarization response time causes the capacitance decrease at the high frequency range for all the samples. The obtained high areal capacitance of HfLaOx is 367 nF/cm2 at 1 kHz. The dielectric constant was calculated to be 24.8.

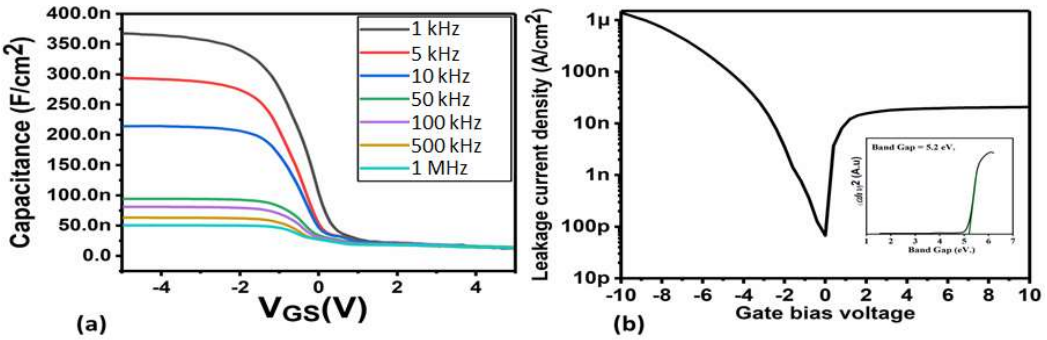

Figure 4.5 At different gate bias voltage (a) Capacitance vs frequency curve (b) Leakage current density curve.

The HfLaOx thin film demonstrates a very low leakage current density of 100 nA/cm^2 at a gate bias voltage of -5 V (**Figure 4.5(b)**). This may be due to the relatively dense, thick, smooth, uniform, and pin-hole free film as described in **Figure 4.3(b)**. The band gap energy extraction of the $HfLaO_x$ thin film was performed utilizing the tauc plot. Inset of **Figure 4.5(b)** illustrates the calculating process for the HfLaOx thin films' band gap energy (5.2 eV). **Figure 4.5(b)** shows the leakage current density plot of $HfLaO_x$ dielectric thin film at various gate bias voltages.

4.4.2. Electrical Properties

Electrical characterization of the produced OFET device was carried out using KEYSIGHT-B1500 semiconducting parameter analyzer, and the device's performance was evaluated using output/drain and transfer characteristics. In order to evaluate the electrical characteristics of the constructed OFET device, certain crucial transistor parameters, including threshold voltage (V_{TH}), and charge carrier mobility (μ_p) were considered from these behavioral curves. For a constant source to gate voltage range (0 to -5 V with a step length of 1) and variable source- drain voltage (V_{DS} = 0 V to -5 V), the output characteristics of the OFET are demonstrated. The output/drain characteristics of the developed FET is displayed in **Figure 4.6(a).** The same way, the gate-source voltage (V_{GS} = 0 V to -5 V) is swept while the source-drain voltage is changed in fixed increments (0 to -5 V with a step length of 1) to plot the device's transfer characteristics (see **Figure 4.6(b)**). The drain current (I_{DS}) of the OFET in the saturation regime was calculated using the following equation. [76]-

$$I_{DS} = \frac{1}{2}\mu_P C_{OX}\frac{W}{L}(V_{GS} - V_{TH})^2 \; ; \; V_{DS} \geq V_{GS} - V_{TH} \tag{4.1}$$

Where V_{TH}, μ_P, W/L, and C_{OX} represent the threshold voltage, mobility, aspect ratio (AR) of the channel, and capacitance per unit area of the dielectric layer respectively. **Equation (4.1**) can be rewritten as:

$$\sqrt{I_{DS}} = \sqrt{\frac{1}{2}\mu_P C_{OX}\frac{W}{L}}(V_{GS} - V_{TH}) = XV_{GS} - Y \tag{4.2}$$

Utilizing the linear fit of **Equation (4.2**), where X and Y are the slope and intercept, respectively, threshold voltage and mobility are retrieved conceptually. The threshold voltage and mobility of the device can be calculated by **Equation (4.3)** as-

$$\mu_P = \frac{2}{AR.C_{OX}}X^2 \;\&\; V_{TH} = \frac{-Y}{X} \tag{4.3}$$

The semiconducting layer and dielectric interface's trap charge carrier density (Δn_{trap}) is

determined by [76]-

$$\Delta n_{trap} = \frac{Q_{trap}}{q} = \frac{\Delta V_{TH} C_{OX}}{q} \quad \textbf{(4.4)}$$

Here Q_{trap} is the trapped charge of the dielectric-semiconductor interface. It is evident that the V_{TH} increases with increasing H_2S gas concentration because H_2S molecules have a tendency to electrostatically trap the holes (q) in the active sensing layer [78], which results in the modulation of the trap charge carrier density and I_{DS} of the OFET. The threshold voltage (V_{TH}) of the developed device noticeably shifts when the analyte concentration changes across the sensing surface, which is further supported by the mathematical relationship represented by **Equation (4.4).** Additional evidence of this phenomena was supplied by the behavioral observation of the charge carrier mobility, which exhibits a sharp decline with rising gas concentration (**Figure 4.8 (b)**). The variation in threshold voltage and trap charge density with hydrogen sulfide concentration is shown in **Figure 4.8(c).**

Table 4.2 lists all the electrical and gas sensing metrics that were retrieved after being exposed to various quantities of H_2S gas.

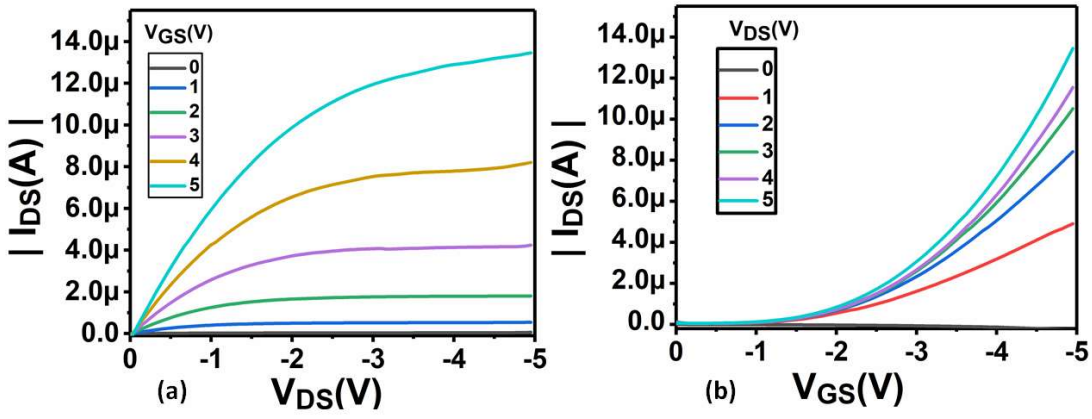

Figure 4.6 (a) Drain characteristics, (b) Transfer characteristics of the fabricated OFET.

4.5 Gas Sensing Properties

4.5.1. Sensor Response

At ambient conditions and room temperature, all measurements were made. The device was exposed to various hydrogen sulphide gas concentrations, and the corresponding transfer characteristic was reported at biassing conditions of V_{GS} = -5 V and V_{DS} = -5 V. In the present work, the operating voltage of the TFT has been optimized with varying dielectric thickness for low voltage operation, i.e.V_{DS} = V_{GS} = -5 V, low leakage current, enhanced I_{DS}, and high dielectric areal capacitance. The gas sensor response of the developed device is extracted at a specific H_2S gas concentration using the drain current (I_{DS}) variation in the transfer characteristics shown in **Figure 4.8(a). Figure 4.8(b)** shows the sensor response of the device for various H_2S gas concentrations. Sensor response has been calculated using [77]-

$$S\% = \frac{\left|I_{DS(AIR)} - I_{DS(GAS)}\right|}{I_{DS(AIR)}} * 100\% \quad \textbf{(4.5)}$$

The OFET device, which displayed a sensor response of roughly 93.2% at 1 ppm, confirmed unprecedented sensitivity.

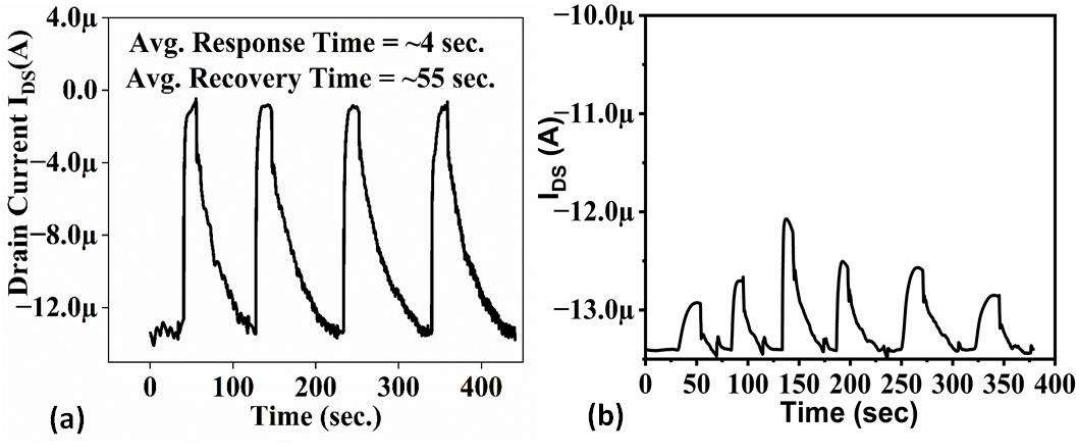

Figure 4.7 (a) Repeatable Response-Recovery behavior of the device (b) Transient behavior of the interfering gases for selectivity analysis

4.5.2. Transient Analysis and Repeatability

Investigations on transient and repeatability were done to remark on the device's response-recovery behavior and repeatability in regard to exposed H_2S gas. Response time is defined as the time required to reach 90 % from 10 % of the final value after gas insertion. Similarly, recovery time is defined as the time required to reach 10 % of the final value from 90 % after gas removal. When the gas ambient is removed, it has been seen that the device fully returns to its baseline level within a set amount of time. **Figure 4.7(a)** shows the sensing device's repeating transient response has been examined over a period of four cycles, and the results show that it has great repeatability and delivers excellent response-recovery behavior towards the H_2S analyte while maintaining almost uniform sensor response. Over a 1 ppm exposure of the H_2S analyte, the device has a response/recovery time of 4/55 sec, respectively.

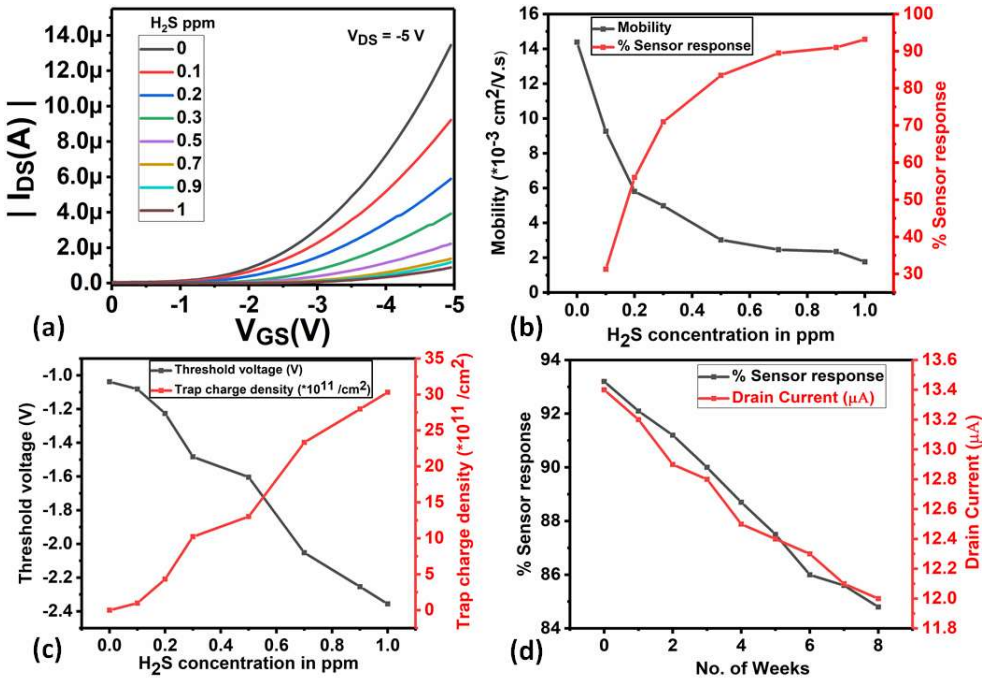

Figure 4.8 (a) The device's drain current variation by varying H_2S concentrations at V_{DS} = -5 V, (b) Sensor Response and mobility variation with varying Hydrogen sulfide gas concentrations, (c) Trap charge density and threshold voltage variation with varying Hydrogen sulfide gas concentrations, (d) Sensor response and drain current change over the weeks.

Table 4.2 OTFT parameters with exposed H_2S gas

H_2S ppm	V_{th} (Volts)	Mobility *10^{-3}(cm^2/V.s)	Trap density (*10^{11}/cm^2)	I_{DS} (μA)	S (%)
0	1.038	14.38	0	13.4	0
0.1	1.081	9.26	0.989	9.2	31.3
0.2	1.226	5.81	4.324	5.9	56
0.3	1.483	4.98	10.235	3.9	71
0.5	1.604	3.02	13.018	2.2	83.5
0.7	2.052	2.46	23.322	1.4	89.5
0.9	2.254	2.35	27.968	1.2	91
1	2.356	1.76	30.314	0.9	93.2

4.5.3. Selectivity

By subjecting the sensor to several interfering gases, including H_2S, NO_2, NH_3, SO_2, H_2, CO, and CO_2, at concentrations of 1 ppm for H_2S and 10 ppm for other gases, the sensor's selectivity was also examined. Interfering gases have been passed sequentially and the

transient performance has been recorded as presented in **Figure 4.7(b).**

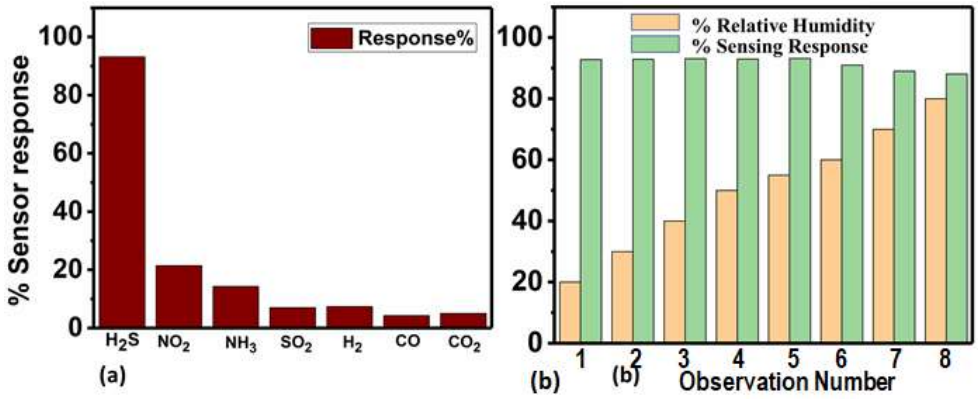

Figure 4.9 (a) Selectivity investigation (b) Sensor response variation with Relative Humidity analysis.

After returning to the baseline another gas has been passed. 1st cycle is for CO, 2nd cycle is for SO_2, 3rd cycle is for NO_2, 4th cycle is for NH_3, 5th cycle is for H_2, and 6th cycle is for CO_2. The response to H_2S is significantly higher than that to the other test gases, as shown by the plotted selectivity in **Figure 4.9(a)**, proving its remarkable selectivity for H_2S detection.

4.5.4. Relative Humidity and Stability

Figure 4.9(b)'s bar graph displays the effect of different humidity investigation on the device's response to H_2S gas exposure. The impact of relative humidity (RH) on the sensitivity of the fabricated sensor was examined across the range of 20-80% RH at 1 ppm of exposed H_2S gas. Over this range, the sensor performs nearly consistently. The developed device's sensitivity did, however, somewhat decrease at increasing relative humidity levels, most likely as a result of water vapor molecules absorbing onto the PCPDTBT sensing film [78]. The film's sensitivity to the exposed analyte is decreased by the water vapour molecules' adsorption because there are less vacant sites for analyte adsorption. Recent published literature[99] has investigated an humidity resistant approach for gas

detection at RT, which we will try to incorporate in the future work. The sensor response variation (at 1 ppm H_2S analyte) and drain current deterioration (without gas exposure) were then measured over an 8-week period to provide yet another evaluation of the sensor's long-term stability. The sensor provided outstanding stability, as shown by the results presented in **Figure 4.8(d)**, with small percentage degradations of about 10.5% and 9% for the sensor response and drain current, respectively.

4.6 Gas Sensing Mechanism

Organic semiconductor's molecular structure, the degree of film alignment, the presence of functional groups in the polymer, surface topography, film thickness, and the grain boundaries of the organic film can all have an impact on an organic thin film's sensing ability [68][79][80][100][101]. All of the above-mentioned metrics have greatly improved, as previously discussed in the sections, and they all help to increase the device performance. PCPDTBT/MoS_2 nanocomposite only contains 5% (w/v) amount MoS_2. Therefore, overall behavior of the nanocomposite is of p-type. Furthermore, using the charge injection (adsorption or physisorption) and charge transport the gas sensing mechanism can be described in two steps; Possible adsorption mechanism as follows:

Due to the presence of two electron-withdrawing imine nitrogen atoms (C=N), BTZ is an especially powerful e- accepting unit. Compared to Sulphur, nitrogen has a substantially higher electronegativity. Sulphur will thus lack electrons and take on a partial negative charge. Additionally, a strong van der Waals force will attract the hydrogen sulphide gas' lone pairs to the Sulphur atom of the BTZ functional group. In the case of CPDT, the Sulphur atom will produce a smaller partial negative charge compared to the Sulphur of the BTZ group since it has somewhat lower electronegativity than carbon. As a result, by

a weak van der Waals force, the lone pairs of hydrogen sulphide gas will bond to the Sulphur atom of the CPDT functional group. The holes in the sensor film will be trapped by these adsorbed or injected electrons. Charge trapping, which occurs as a result, decreases the carrier density and drain current in the sensing film. Due to the lack of available unoccupied adsorption sites, I_{DS} has a tendency to stabilize once the number of H_2S molecules adsorbed on the sensing surface reaches saturation. When the sensing material is exposed to air once again or the gas ambience is removed, the adsorbed H_2S molecules progressively desorb, raising the I_{DS}. I_{DS} steadily returns to its initial level once H_2S molecules are removed from the sensing film. Perhaps weak van der Waals force adsorption sites experience desorption first, followed by strong adsorption sites, leading to a longer recovery time than response time. Now, the possible charge transport mechanism as follows:

We will first describe how charges are transported in pristine PCPDTBT chain, and then we will describe how charges are transported in a composite film. The conductive channels created by the mutually overlapping orbits of the PCPDTBT rings serve as the means by which charge is transported along the PCPDTBT film. The intrachain and interchain transport methods can be used to explain the charge transfer process. The matrix of interconnected individual polymer chains may be used to visualize polymer film. Due to the improved molecular ordering of the sensing film, intrachain processes account for the majority of charge transmission. Where the polymer chains are disorganized, interchain movement occurs [75]. **Figure 4.10** depicts the intrachain and interchain transport mechanisms. The high mobility throughout the extended backbone of polymer chains from crystallite to crystallite is anticipated to be promoted by straight tie chain intercrystallite connections (also known as interchain coupling), which join two polymer chains together

using high order alkyl side chains. High levels of interchain packing assist conjugated polymers for charge carrier localization via interchain transport process when disordered areas and amorphous phases are present around the crystallite domains [75]. Let's now discuss the composite film's charge transfer method. To create charge carriers in the polymer chain by charge exchange with the dopant species, a polymer's structure must be chemically modified through doping. The addition of the dopant MoS_2 to the polymer backbone also affects how the positive charge is distributed overall. The attraction force between the nucleus of one repeat unit and the electron of the other repeat unit causes carrier delocalization along the polymer chain, which leads to carrier movement via intra and interchain transport processes [96].

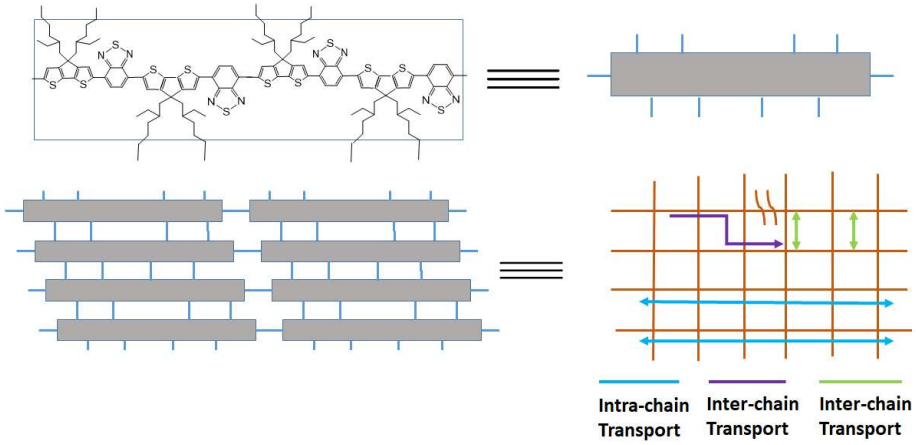

Figure 4.10 Charge carrier transport in polymer backbone.

These dopants are categorized as primary dopants since they alter the conductivity of the polymer as well as its electrical, structural, magnetic, and optical characteristics. A secondary dopant (H_2S analyte in this case) is considered as a substance that upon exposure to a primary-doped polymer, alters the inherent properties. In PCPDTBT/ MoS_2 hybrid nanocomposites, it is possible to interpret the altered hole transport properties in terms of

charge transfer-type interactions between the PCPDTBT host and MoS_2 guest, which include an increase in trap density and characteristic trap energy as well as an improvement in hole mobility. Nevertheless, the rise in charge carrier mobility raises the possibility that charge transfer complexes (CTCs) will serve as the primary method for interaction between the host and guest. The guest MoS_2 NPs may induce desirable energy states that will affect the host PCPDTBT band gap. As seen in **Figure 4.11(b),** these advantageous energy states within the band gap are referred to as traps, which further leads to a rise in trap density and characteristic trap energy. MoS_2 NPs offer additional decaying paths for the excited carriers through the trap states. Therefore, the MoS_2 NPs facilitate the charge carriers' transportation throughout the PCPDTBT film, enhancing charge carrier mobility (**Figure 4.11(a)**). Previously, the charge carriers had to traverse from one polymer chain to another. Thus, compared to pristine polymer thin films, charge carriers may flow more readily in PCPDTBT/ MoS_2 composite thin films. As a result, the introduction of MoS_2 NPs increases the hole mobility in PCPDTBT.

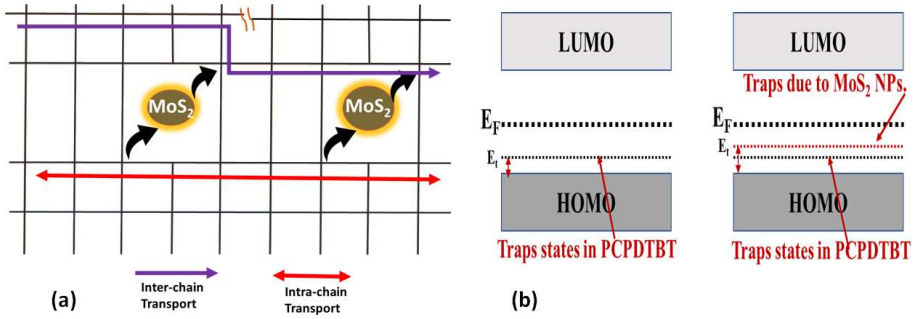

Figure 4.11 (a) Charge carrier transport in polymer nanocomposite matrix (b) Distribution of traps energy states with-in the band gap of PCPDTBT and PCPDTBT/ MoS_2.

With the aid of redox centers, the nanocomposite film may be seen as a matrix that facilitates carrier transport (**Figure 4.11(a)**). As previously mentioned, the surface topology

and electrical characteristics of the sensing film are further altered when the secondary dopant/analyte being detected forms a charge transfer complex with the analyte. Due to the minimal force of interaction (Van der Waals) involved, the alteration of the sensing film's electrical characteristics is reversible, and enables for complete device recovery and exhibit gas sensor's outstanding repeatability and reversibility.

4.7 Conclusion

As stated in the abstract of this chapter, it is necessary to develop the sensor to operate at low voltage. To solve this problem, in this chapter the SiO_2 dielectric layer has been replaced by high-k dielectric material HfLaOx. In this regard, HfLaOx gate oxide exhibits excellent dielectric properties and demonstrates enormous potential for low voltage operable OFETs. The device also provides outstanding repeatability, response-recovery behavior, stability against ambient and humidity conditions, and sensor response. The floating film transfer method has a number of benefits, including superior film morphology, low cost, self-alignment of the film, solution processibility, large area fabrication, and good charge transport with an improved sensing response of the manufactured sensor. Additionally, photoirradiation of composite solution and the solvent vapor annealing method provides better charge injection, higher crystallinity, and a charge transfer mechanism throughout the polymer chain, which enhances the response/recovery properties of the developed device. The fabricated sensor has outperformed the sensors developed in previous chapters and exhibits an excellent sensing response of ~93%, a response/recovery time of 4/55 sec over 1 ppm exposure of H_2S gas, and is almost independent of relative humidity variation with good ambient stability. The developed OFET's excellent combination of high sensitivity, repeatability, fast response, and complete recovery after

removing the gas ambience makes it possible to use it as an H_2S sensor in real gas monitoring systems. In conclusion, the manufactured sensor may be used in real-time, low-cost H_2S gas detecting applications with sub-ppm range detection capabilities.